Yun Hsu
e-mail: yhsu@jaycor.com

Christopher E. Brennen
e-mail: brennen@caltech.edu

California Institute of Technology,
Mail Code 104-44,
Pasadena, CA 91125

Effect of Swirl on Rotordynamic Forces Caused by Front Shroud Pump Leakage

Unsteady forces generated by fluid flow through the impeller shroud leakage path of a centrifugal pump were investigated. The effect of leakage path inlet swirl (pump discharge swirl) on the rotordynamic forces was re-examined. It was observed that increasing the inlet swirl is destabilizing both for normal and tangential rotordynamic forces. Attempts to reduce the swirl within the leakage path using ribs and grooves as swirl brakes showed benefits only at low leakage flow rate. [DOI: 10.1115/1.1511164]

1 Introduction

Previous experimental and analytical results have shown that discharge to suction leakage flows in the annulus surrounding a shrouded centrifugal pump contribute substantially to the fluid induced rotordynamic forces ([1,2]). Experiments conducted in the Rotor Force Test Facility (RFTF) at Caltech on an impeller undergoing a predetermined whirl motion have shown that the contributions to the normal and tangential forces from the leakage flows can be as much as 70% and 30% of the total, respectively ([3]). Other experiments ([4]) examining the consequences of leakage flows have shown that the rotordynamic forces are functions not only of whirl ratio, but also of the leakage flow rate and the impeller shroud to pump housing clearance. The magnitude of rotordynamic forces were found to be inversely proportional to the clearance. A region of forward subsynchronous whirl was found for which the average tangential force was destabilizing.

Guinzburg et al. [5] examined the difference in rotordynamic forces with and without a prescribed inlet swirl at entrance to the leakage path. The tangential force increased in the presence of inlet swirl, and hence the effect of inlet swirl was found to be destabilizing. Uy and Brennen [6] continued the work and did a parametric evaluation of the effect of inlet swirl. Later studies by Sivo et al. [7] examined the effectiveness of antiswirl brakes in reducing the destabilizing region of forward whirl.

Subsequent to the tests reported by Uy and Brennen, detailed comparison of the leakage path pressure profiles strongly suggested that the inlet swirl velocities were not consistent with the inclination of the inlet swirl vanes as assumed by Uy and Brennen. The present paper presents data in which the inlet swirl was measured; this requires a reassessment of the effect of inlet swirl on the rotordynamic coefficients. Also examined are the effects of antiswirl brakes as well as antiswirl grooves within the leakage pathway.

2 Rotordynamic Forces

Figure 1 shows a schematic of the hydrodynamic forces that act on a rotating impeller whirling in a circular orbit. The unsteady fluid forces (which are functions of rotor displacement) acting on the impeller due to the imposed whirl motion (eccentricity ε, whirl frequency Ω) are decomposed into a force normal to the direction of whirl motion, F_n, and a force in the direction of forward whirl motion, F_t. (Force moments would also occur from rotor displacement, see Tsujimoto et al. [8].) The normal and tangential forces are traditionally presented in dimensionless form as functions of the whirl frequency ratio, Ω/ω. Typical data for F_n and F_t from the present measurements is shown in Fig. 2.

It is convenient for rotordynamicists to fit F_n to a quadratic function of the whirl frequency ratio, Ω/ω, and to fit the dimensionless tangential force, F_t, to a linear function as shown in Fig. 2. The appropriate expressions are

$$F_n = M\left(\frac{\Omega}{\omega}\right)^2 - c\left(\frac{\Omega}{\omega}\right) - K; \quad F_t = -C\left(\frac{\Omega}{\omega}\right) + k \tag{1}$$

where the dimensionless coefficients are the direct added mass (M), direct damping (C), cross-coupled damping (c), direct stiffness (K), and the cross-coupled stiffness (k). It should be noted that the fluid-induced forces may not always conform to these simple functions of the whirl frequency ratio. However, this assumption is common in the rotordynamics literature. Brennen [9] and Jery [3] contain more detailed discussions of the derivation of Eqs. (1), and the process for experimentally measuring the forces. In the present work all five force coefficients were directly evaluated from the curve fits to the graphs of F_n and F_t.

For rotor stability, a positive normal force F_n will cause the eccentricity to increase and hence be destabilizing. From Eqs. (1), a large negative direct stiffness at zero whirl frequency ($\Omega/\omega = 0$) would correspond to such a case. When Ω/ω is positive, a positive tangential force F_t would also be destabilizing as this would drive the forward whirl motion.

A convenient measure of the rotordynamic stability is the ratio of cross-coupled stiffness to the direct damping (i.e., k/C) which is conventionally termed the whirl ratio. This defines the range of positive subsynchronous whirl frequency ratios, $0 < \Omega/\omega < k/C$, for which the tangential force is destabilizing.

3 Test Apparatus

The present experiments were conducted in the Rotor Force Test Facility (RFTF) at Caltech [3]. The leakage flow test section of the facility is schematically shown in Fig. 3. The intention is to isolate the leakage flow forces by using a solid rotor and to generate the flow through the leakage path by an auxiliary pump. The main components of the test section apparatus consist of the solid rotor, a stator (the stationary shroud), the rotating dynamometer (or internal force balance), an eccentric whirl mechanism and a leakage exit seal ring. The working fluid is water. An inlet guide vane is used for the tests with inlet swirl and is illustrated in Fig. 3.

The rotor is mounted directly to the rotating dynamometer, which in turn is connected to a data acquisition system that permits measurements of the rotordynamic force matrix components ([3]). The eccentric drive mechanism imposes a circular whirl orbit on the main shaft rotation. The radius of the whirl orbit (eccentricity) can be varied but this set of experiments used one

Contributed by the Fluids Engineering Division for publication in the JOURNAL OF FLUIDS ENGINEERING. Manuscript received by the Fluids Engineering Division August 17, 2001; revised manuscript received May 6, 2002. Associate Editor: Y. Tsujimoto.

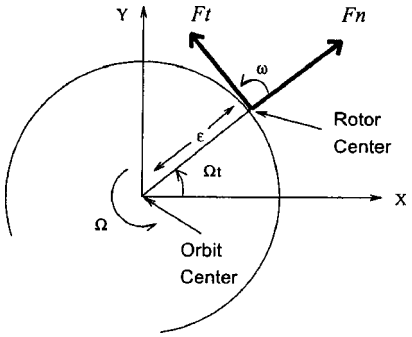

Fig. 1 Schematic of the fluid-induced forces acting on an impeller whirling in a circular orbit

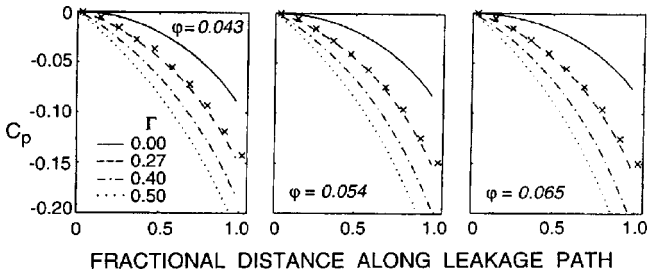

Fig. 4 Comparison of the experimental measurements (×) of the pressure coefficient (C_p) profiles in the leakage path for $\phi = 0.043$, 0.054, and 0.065 with the calculated profiles for inlet swirl ratios of 0, 0.27, 0.4, and 0.5

eccentricity, $\varepsilon = 0.025$ cm. The seal ring at the leakage exit models a wear ring. The clearance between the face seal and the impeller face is adjustable, but was set to 0.050 cm for these tests. The tested leakage flow rate ranged up to 1.15 l/s. The temperature drift of the dynamometer electronics is postulated to be the largest contributor to force measurement errors. The uncertainties were evaluated experimentally and in all reported rotordynamic force coefficients were 5% with the exception of the direct stiffness, K, for which the uncertainty was 8%. The uncertainty in the measurement of the flow rate was 1%.

The experimental configuration with the rotor and stator forming the leakage path is shown in Fig. 3. The two rotor/stator configurations referred to in this paper (the so-called conical and contoured rotor geometries) were described and used by Uy and Brennen [9]. The present tests used primarily the contoured rotor which has an eye-to-tip diameter ratio of 0.454, tip diameter of 18.73 cm, and an axial length of 4.29 cm. The rotor was designed using a third-order polynomial with the contour parallel to the centerline at the eye and perpendicular to the centerline at the tip. The matching stator was constructed to maintain a constant clearance, $H = 0.30$ cm, normal to the surfaces. The conical rotor has a 45-deg leakage path and has the same tip radius and the same tip-to-eye diameter ratio as the contoured rotor. An axial clearance device that models a face seal on a centrifugal pump is used. The inner radius of the seal is 3.30 cm, and its clearance is set to 0.05 cm for all tests. The effect of inlet swirl was investigated by installing guide vanes at the leakage inlet to introduce pre-rotation in the direction of shaft rotation. Figure 3 shows a typical vane consisting of a logarithmic spiral channel with a turning angle of six deg. A series of vanes with angles $\alpha = 1$ deg, 2 deg, and 6 deg were fabricated. The swirl ratio, Γ (the ratio of the leakage flow circumferential velocity to the impeller tip velocity at inlet to the leakage path) is varied by changing the inlet leakage flow rate and the turning angle. Another inlet guide plate with a set of 24 radial vanes designed to eliminate inlet swirl. The swirl ratio depends on the flow coefficient and turning angle, α, according to $\Gamma/\phi = H/B \tan\alpha$ where $B = 0.318$ cm is the width of the logarithmic spiral channel. A derivation of this relation (which assumes all leakage flow is constrained to follow the vane) is found in Guinzburg et al. [5]. The relation was assumed by Uy and Brennen [6] in their presentation of the effects of inlet swirl on rotordynamic forces.

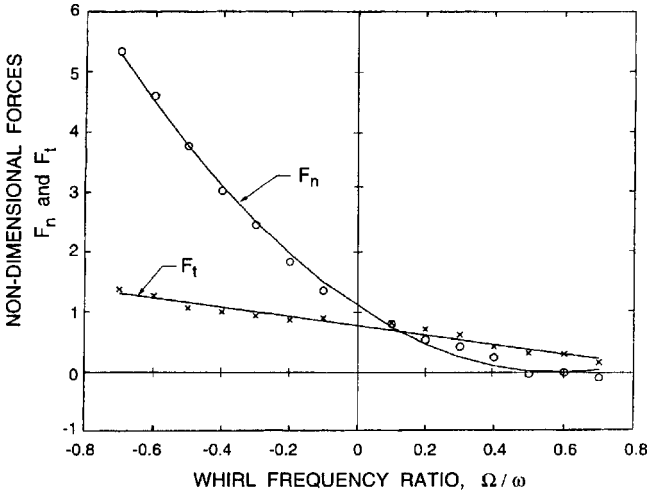

Fig. 2 Typical nondimensional data for F_n and F_t from the current experiments as functions of the whirl frequency ratio Ω/ω (data for contoured rotor with inlet swirl at $\phi = 0.043$)

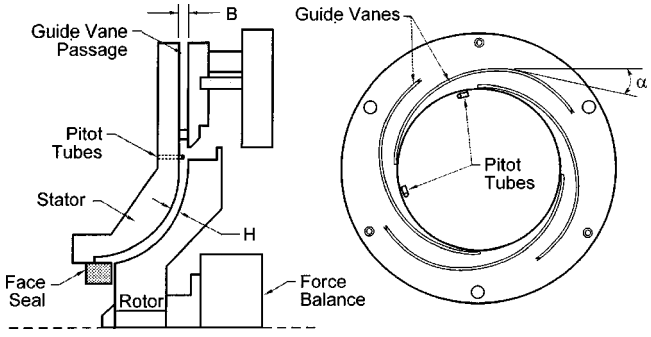

Fig. 3 Schematic of the experimental facility showing the rotor and stator assembly (left), the $\alpha = 6$ deg inlet guide vanes (right) and the location of the Pitot tubes

However, during investigations of the leakage flow field, questions arose concerning the inlet velocities to the leakage path. One source of these questions were comparisons between experimentally measured leakage path pressure distributions and those calculated theoretically. We digress here to cover this issue.

4 Leakage Path Pressure Distributions

We present the pressure profile comparisons which led to the need for inlet swirl measurements (for full details see [10]). The pressure profiles inside the leakage path were examined both experimentally and computationally for the conical impeller fitted with the inlet guide vanes. The computations were done using the new vorticity method for solving the Childs' bulk flow equations ([10]). (Using the original Childs' perturbation method yields qualitatively similar results.) Pressure taps drilled through the stator of the conical impeller provided water manometer measurements for profiles of three different flows, $\phi = 0.043$, 0.054, and 0.065, using the 6 deg inlet guide vane, which was designed to provide inlet swirl ratios of 0.4, 0.5, and 0.6, respectively, at each of those flow rates. Experiments were conducted with the rotor eccentric but not whirling ($\Omega/\omega = 0$). The resulting pressure coefficient distributions are presented in Fig. 4; it can be seen that

the experimental pressure profiles, referenced to the pressure at inlet to the leakage path, are nearly identical for the three flows. Computationally the inlet swirl was the only parameter which affects the pressure profile significantly. As seen in Fig. 4, in all three flows the pressure profiles are best matched by setting the inlet swirl ratio in the computations to 0.25–0.27 of the rotor tip speed. This finding motivated the inlet swirl measurements and confirmed the suspicion that the inlet swirl was nearly the same for all of the inlet guide vanes regardless of the flow rate. Since there are only slight differences in the inlet structure of the conical and contoured rotors, the same conclusion applies to the contoured rotor.

5 Inlet Swirl Measurements

Motivated by the preceding results, Pitot tubes were installed to measure the flow velocities at inlet to the leakage path. Considerations were given to using five-hole Pitot tubes. This was not done, however, for several reasons. The flow velocities are likely to vary with distance from the walls. This would mean that several measurements at different distances from the walls would be needed to accurately assess the flow, a difficult feat considering the narrow spaces in the apparatus. In addition the flow is unsteady and highly disturbed, making the accuracy of the flow angle measurements a concern. Because of this, it was decided that a cruder measurement of the velocity in the tangential direction would suffice for the purposes of ascertaining the inlet flow conditions to the leakage path.

The stator had two holes drilled for insertion of the Pitot tubes, as shown in Fig. 3. The Pitot tubes were placed immediately after the exit of the inlet guide vanes and before the entrance to the leakage path, a gap of approximately 0.8 cm normal to the axis of rotation. Normally one would have the diameter of the Pitot tube be less than one quarter of the gap. The Pitot tubes were fabricated from 0.3 cm diameter stainless steel tubing. Their diameter is therefore comparable to the leakage path clearance and the width of the inlet guide vanes. The tubes were connected to the set of water manometer mentioned earlier for stagnation pressure readings. Existing pressure taps next to the Pitot tubes were used for static pressure measurements. The difference between the readings is the velocity head of the flow in the direction facing the Pitot tube.

In most of the tests only the swirl velocity was measured by setting the Pitot tubes tangent to the circumference. Changing their orientation to face the flow directly did not change the measurements, as the difference was within the uncertainties. Because of the large diameter of the Pitot tubes compared to the gap width, the measured velocities are likely to be some average value of the velocity in the circumferential direction near the inlet to the leakage path. Though the measurements of the swirl velocity may be imprecise, confidence in the results was bolstered by the agreement between the measured pressure profiles and those calculated using the measured inlet swirl ([10]).

Figure 5 shows that the inlet swirl vanes did not work as designed; they almost all provided about the same inlet swirl. On the other hand, the radial vanes *did* prevent inlet swirl at higher flow rates. These velocity measurements are consistent with theoretical predictions from the bulk flow model ([10]). It is postulated that inside the small clearance in the guide vane structure, viscous forces dominate and they act to slow the flow in the circumferential direction and expel the fluid in a more radial manner at the exit from the guide vanes. Also some mixing may occur inside the region between the end of the inlet guide vanes and the beginning of the leakage path and would reduce the effects of inlet swirl vanes.

Since the entrance regions of the contoured and the conical geometries are very similar, there is no reason to expect their inlet swirls would be different.

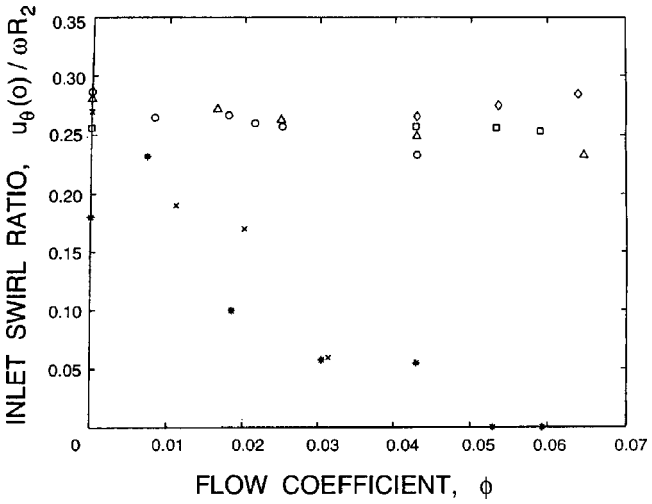

Fig. 5 Experimental inlet swirl ratio versus flow coefficient ϕ, with 6-deg inlet swirl vanes at 500 rpm(◇), 1000 rpm(□), with 2-deg swirl vanes at 500 rpm(△), 1000 rpm(○), and with radial vanes at 1400 rpm(×) and 1000 rpm(*)

6 Effects of Inlet Swirl

Uy and Brennen [6] performed a set of experiments to determine the effects of inlet swirl on the unsteady rotordynamic forces on the contoured impeller. Different inlet swirl angles were employed to alter the inlet swirl ratio, and a swirl vane with radial channels was used to generate data for zero inlet swirl. The flow coefficients ranged from $\phi = 0.01$ to 0.066 using flow rates from 0.17 to 1.15 l/s at 1000 rpm. The Reynolds numbers for $\phi = .055$ were $\mathrm{Re}_\omega = 27170$ and $\mathrm{Re}_{u_s} = 1494$. Uy and Brennen assumed the inlet swirl was consistent with the angles of the inlet guide vanes and therefore published Fig. 6, which showed that for nonzero inlet swirl, the magnitude of the inlet swirl, Γ, did not affect the rotordynamic forces.

However, the later comparison of pressure profiles led to questions concerning the accuracy of the assumed inlet swirl in the experiments ([10]). Subsequently, the Pitot tube measurements of inlet swirl velocities did show that the assumed swirl velocities were indeed incorrect. Figure 7 presents the corrected experimental data, showing only two inlet swirl ratios, evaluated using the correct, measured values of the swirl. It shows that the effect of swirl is destabilizing, as K becomes larger in negative magnitude and k/C increases. The coefficients representing the tangential forces, C and k, become larger with increasing swirl. At higher flow coefficients, $\phi > 0.03$, no discernible trends can be observed in the rotordynamic coefficients for constant swirl.

However, the general comments made by Uy and Brennen on the effect of swirl are still valid. For the coefficients which determine the normal force, M, c, and K, the added mass does not exhibit an appreciable difference in the cases with and without swirl. The magnitude of the direct stiffness is higher and the magnitude of the cross-coupled damping is smaller with no inlet swirl. In summary, the circumferential fluid velocity induced by inlet swirl affects the rotordynamic behavior significantly, especially the whirl ratio, which defines the range where tangential forces are destabilizing.

The combined effect of inlet swirl and leakage path geometry was also investigated. Figure 8 presents the rotordynamic force coefficients for both the contoured and conical leakage path geometry, updated with the measured inlet swirls. The coefficients of the normal force appear to be similar, but there are significant differences in the trends and magnitudes of the cross-coupled stiffness and direct damping, leading to substantial differences in

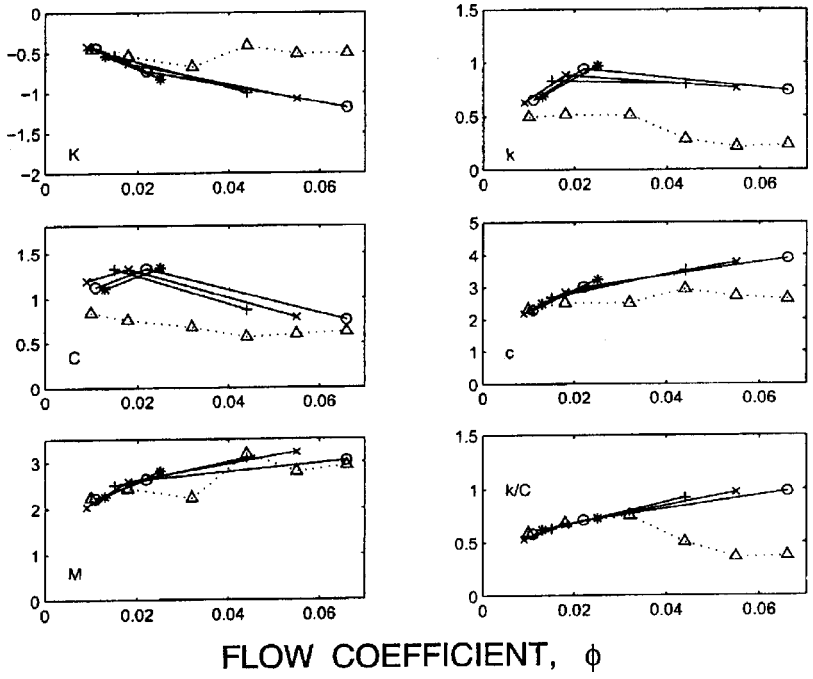

Fig. 6 Experimental rotordynamic coefficients for the contoured rotor plotted against flow coefficient, ϕ, for tests with inlet swirl, $\Gamma=0.0$ (△), 0.4 (+), 0.5 (×), 0.6 (○) and 0.7 (*) (presented by Uy and Brennen [6] and here shown to be inaccurate)

the whirl ratio. The contoured rotor exhibits an increasing whirl ratio with increasing flow rate, while the conical rotor exhibits the opposite trend.

7 Antiswirl Ribs and Grooves

We now shift attention from inlet swirl to swirl reduction in the leakage path by vanes installed within the passage. Previous investigations ([7]) demonstrated some benefits from fitting antiswirl ribs to the surface of the stator; they decreased the destabilizing forces. The inner surface of the conical stationary shroud was designed to accept meridional ribs or swirl brakes along the length of the leakage path. As shown in Fig. 9, four equally spaced ribs, 0.5 cm wide and 0.16 cm high, were installed for these tests. The effectiveness of cutting grooves on the stator sur-

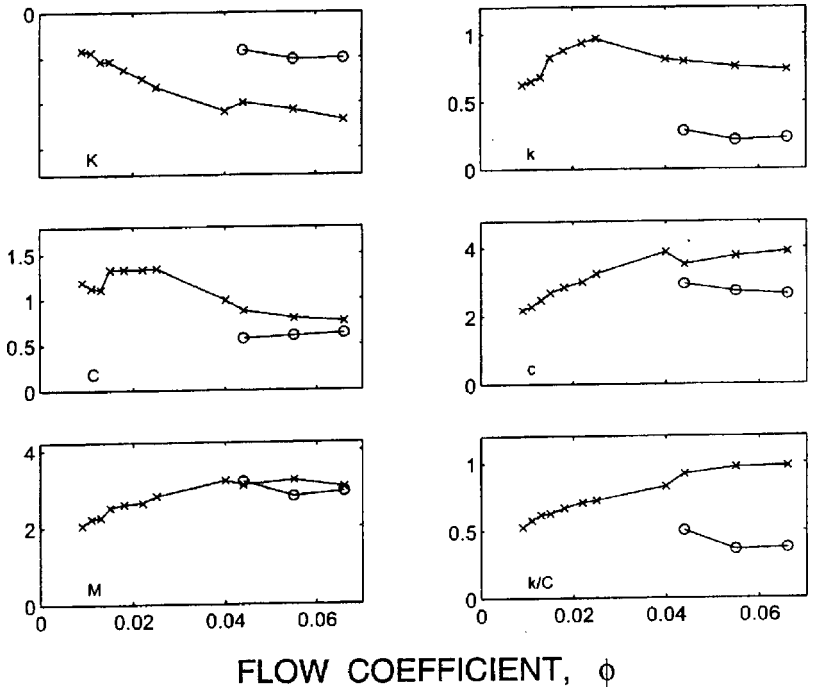

Fig. 7 Experimental rotordynamic coefficients for the contoured rotor plotted against flow coefficient, ϕ, for tests with inlet swirl, $\Gamma=0.0$, (○) and 0.26 (×)

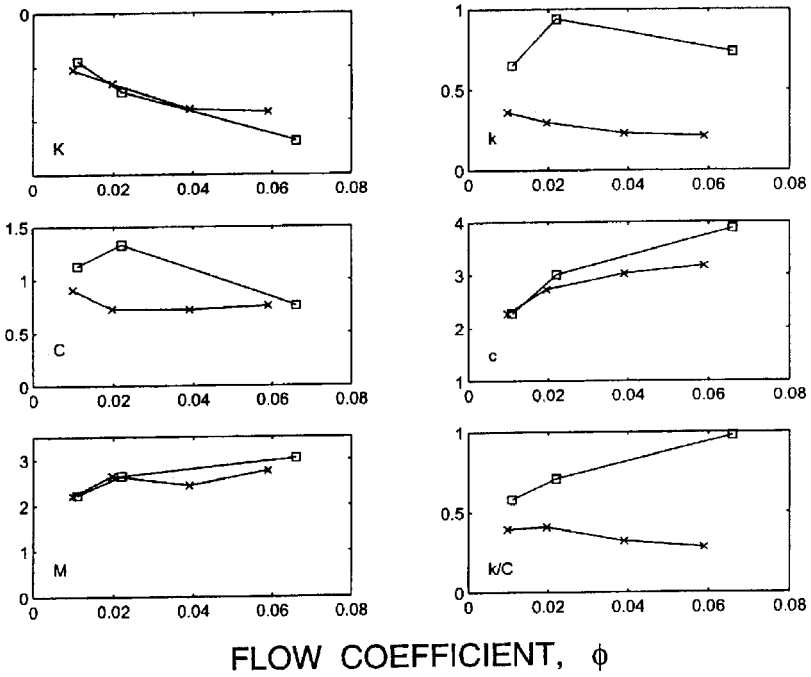

Fig. 8 Experimental rotordynamic coefficients plotted against flow coefficient ϕ for tests with inlet swirl with the contoured rotor ($\square, \Gamma = 0.27$) and the conical rotor ($\times, \Gamma = 0.27$)

face was also examined; the grooves duplicated the height and width of the brakes.

With a rotating impeller, fluid swirl is obviously generated in the leakage path, and the question arises as to how reducing this swirl will affect rotordynamic forces. Therefore, the effects of antiswirl ribs and grooves in the leakage path were investigated. Work by Sivo [7] identified some benefits to having antiswirl ribs in the leakage path, but only for very small flow coefficients.

Figure 10 shows the rotordynamic force coefficients as functions of the flow coefficient for the conical impeller and shroud. The tests were conducted with a 2-deg inlet swirl vane and compare the effects of antiswirl ribs and grooves.

Note that the magnitude of the direct stiffness K is smallest for the tests with no antiswirl devices. Thus in so far as the direct stiffness is concerned, the stability improves with grooves and even more with antiswirl ribs. However the cross-coupled damping coefficient does not show such changes, and the added mass remains about the same for all three cases.

The direct damping of the tangential forces has the same magnitude for all three cases, while the cross-coupled stiffness exhibits different trends. It decreases with flow coefficient with no swirl reduction devices, and increases in the presence of antiswirl ribs. With grooves, the cross-coupled stiffness first increases and then decreases with flow coefficient. This leads to improvements in the whirl ratio for antiswirl devices at low flow coefficients, but to a detrimental effect at higher flow rates. The whirl ratio for the case with antiswirl ribs is increasing with flow coefficient, in marked contrast to the decreasing trend when no antiswirl devices are present.

Thus it seems that antiswirl devices provide some benefit in reducing the destabilizing region in the tangential forces only for very small flow rates. They contribute to an increase in direct stiffness, helping the stability of normal forces.

8 Discussion

Experimental data show that as with annular seals, the rotordynamic forces from front shroud leakage flows in pumps are significantly affected by inlet swirl; an increase in the inlet swirl is destabilizing for both the normal and tangential forces. This observation agrees qualitatively with trends predicted from bulk flow computations. Reduction of inlet swirl provides significant benefits for rotordynamic stability.

As the effects of inlet swirl are destabilizing, reducing the swirl inside the leakage path might seem a beneficial strategy. The results, however, were mixed. At lower flow coefficients, swirl re-

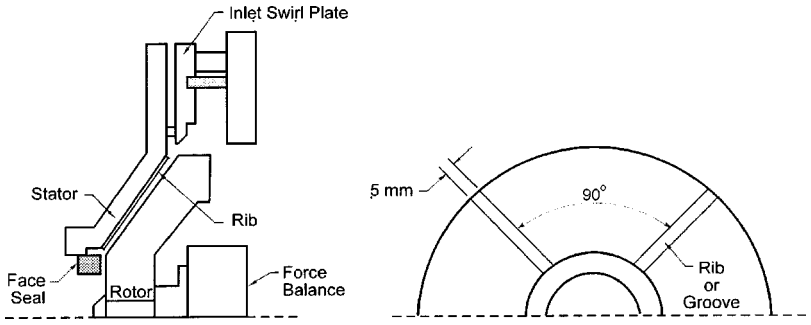

Fig. 9 Swirl reduction devices

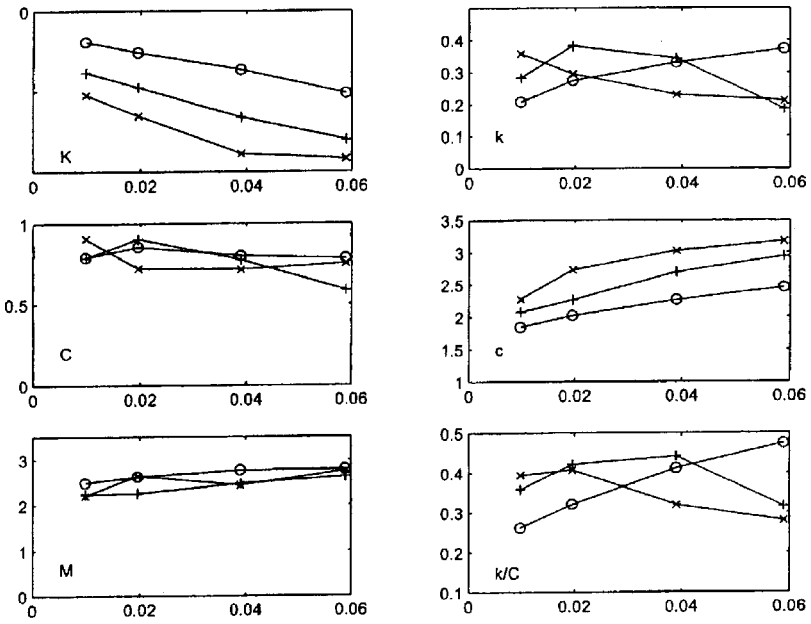

Fig. 10 Rotordynamic coefficients plotted against flow coefficient for experiments with inlet swirl: no antiswirl devices (×), four full-length antiswirl ribs (○), four full-length antiswirl grooves (+).

duction offered some benefit. However, at higher flow rates, the antiswirl devices reduced the unstable normal forces but increased the destabilizing tangential forces.

Nomenclature

B = width of inlet channel and swirl vane
C = direct damping normalized by $\rho\pi\omega R_2^2 L$
C_p = pressure coefficient, $\Delta p/\rho\omega^2 R_2^2$
c = cross-coupled damping normalized by $\rho\pi\omega R_2^2 L$
F_n = force normal to whirl orbit/$\rho\pi\omega^2 R_2^2 L\varepsilon$
F_t = force tangent to whirl orbit/$\rho\pi\omega^2 R_2^2 L\varepsilon$
H = clearance between impeller shroud and housing
K = direct stiffness normalized by $\rho\pi\omega^2 R_2^2 L$
k = cross-coupled stiffness normalized by $\rho\pi\omega^2 R_2^2 L$
k/C = whirl ratio
L = axial length of the leakage path
M = direct added mass normalized by $\rho\pi R_2^2 L$
Q = volumetric leakage flow rate
R_2 = radius of rotor and leakage path inlet, 9.366 cm
Re_ω = Reynolds number, $R_2\omega H/\nu$
Re_{u_s} = Reynolds number, $u_s H/\nu$
Re_{u_θ} = Reynolds number, $u_\theta H/\nu$
u_s = mean leakage throughflow velocity, $Q/2\pi R_2 H$
u_θ = mean swirl velocity at the leakage path inlet
α = angle of logarithmic spiral swirl vane
Δp = static pressure minus pressure at leakage inlet
Γ = leakage inlet swirl ratio, $u_\theta/\omega R_2$
ε = eccentricity of whirl orbit
ν = kinematic viscosity
ρ = fluid density
ϕ = leakage flow coefficient, $u_s/\omega R_2$
ω = main shaft radian frequency
Ω = whirl radian frequency
Ω/ω = whirl frequency ratio

References

[1] Adkins, D., and Brennen, C. E., 1988, "Analysis of Hydrodynamic Radial Forces on Centrifugal Pump Impellers," ASME J. Fluids Eng., **110**, pp. 20–28.
[2] Bolleter, U., Wyss, A., Welte, I., and Sturchler, R., 1987, "Measurement of Hydraulic Interaction Matrices of Boiler Feed Pump Impellers," ASME J. Vib., Acoust., Stress, Reliab. Des., **109**, pp. 144–151.
[3] Jery, B., 1986, "Experimental Study of Unsteady Hydrodynamic Force Matrices on Whirling Centrifugal Pump Impellers," Ph.D. thesis, California Institute of Technology, Pasadena, CA.
[4] Guinzburg, A., 1992, "Rotordynamic Forces Generated By Discharge-to-Suction Leakage Flows in Centrifugal Pumps," Ph.D. thesis, California Institute of Technology, Pasadena, CA.
[5] Guinzburg, A., Brennen, C. E., Acosta, A. J., and Caughey, T., 1993, "The Effect of Inlet Swirl on the Rotordynamic Shroud Forces in a Centrifugal Pump," ASME J. Eng. Gas Turbines Power, **115**, pp. 287–293.
[6] Uy, R., and Brennen, C. E., 1999, "Experimental Measurements of Rotordynamic Forces Caused by Front Shroud Pump Leakage," ASME J. Fluids Eng., **121**, pp. 633–637.
[7] Sivo, J., Acosta, A. J., Brennen, C. E., and Caughey, T. K., 1995, "The Influence of Swirl Brakes on the Rotordynamic Forces Generated by Discharge-to-Suction Leakage Flows in Centrifugal Pumps," ASME J. Fluids Eng., **117**, pp. 104–108.
[8] Tsujimoto, Y., Yoshida, Y., Ohashi, H., and Ishizaki, S., 1997, "Fluid Force Moment on a Centrifugal Impeller in Precessing Motion," ASME J. Fluids Eng., **119**, pp. 366–371.
[9] Brennen, C. E., 1994, *Hydrodynamics of Pumps*, Concepts ETI and Oxford University Press, Oxford, UK.
[10] Hsu, Y., 2001, "Rotordynamic Forces Generated by Annular Leakage Flows in Centrifugal Pumps," Ph.D. thesis, California Institute of Technology, Pasadena, CA.